Investigation on Material Response of 55% SiC_p/Al Composites Induced by Pulsed Laser

HU Maoshun[1], *ZHAO Guolong*[1*], *LI Liang*[1], *ZHANG Xiaohui*[2], *ZHANG Kaihu*[2], *ZHAO Wei*[1]

1. College of Mechanical and Electrical Engineering, Nanjing University of Aeronautics and Astronautics, Nanjing 210016, P.R. China;
2. Beijing Spacecrafts, Beijing 100094, P.R. China

(Received 2 June 2020; revised 7 July 2020; accepted 25 August 2020)

Abstract: Silicon carbide particle reinforced aluminum matrix composites (SiC_p/Al composites) are widely used in aviation, aerospace and electronic package. However, low machining efficiency, severe tool wear and poor surface quality are severe during the machining of SiC_p/Al composites. Laser-induced oxidation is capable to improve the machinability of SiC_p/Al composites. The material response of 55% (volume fraction) SiC_p/Al composites induced by a nanosecond pulsed laser is studied. A metamorphic layer which is composed of an oxide layer and sub-layer is produced. The effects of reaction surrounding and laser average power on the microstructure and thickness of the oxide layer and sub-layer are investigated. Experimental results show that: A thicker oxide layer and a sub-layer are formed in an oxygen-rich atmosphere. The oxides are mainly composed of $2Al_2O_3 \cdot SiO_2$ (mullite). A positive correlation between the laser average power and thicknesses of oxide layers and sub-layers is found. A loose oxide layer of 138 μm and a sub-layer of 21 μm are formed at the laser average power of 6 W, laser scanning pitch of 10 μm, and laser scanning speed of 1 mm/s under an oxygen-rich atmosphere. The high efficient machining of SiC_p/Al composites can be realized by laser-induced oxidation.

Key words: microstructure; oxidation behavior; SiC_p/Al composites; ytterbium-doped pulsed fiber laser

CLC number: TB33; TH140.7 **Document code:** A **Article ID:** 1005-1120(2020)S-0049-09

0 Introduction

Silicon carbide particle reinforced aluminum matrix (SiC_p/Al) is a metal matrix composites which has numerous advantages, such as high wear-resistance, high specific strength, high specific stiffness, good size stability, low coefficient of thermal expansion (CTE), and high damping capacity[1]. These properties make it suitable candidate for precision and microstructural applications, such as micro slots and micro mold of high quality and precision regarding respect ratio and wall angle[2]. Thus, the precise machining of SiC_p/Al composites has great potential.

Owing to the hardness and anisotropy of SiC_p/Al composites, micromachining of SiC_p/Al composites still has great challenges[3]. Wang et al.[4] reported several kinds of surface defects in micro-wire electrical discharge machining (MWEDM) of SiC_p/Al composites. Abrasive waterjet (AWJ) micromachining is an efficient and clean machining process without tool wear and thermally affected zones[5]. However, it acquires high surface quality and high equipment costs. Laser micro machining (LMM) is efficient and versatile to almost all kinds of materials which has numerous advantages such as non-contact, easiness to control, and high dimensional accuracy[6-7]. Despite these advantages, heat-affected

*Corresponding author, E-mail address: zhaogl@nuaa.edu.cn.

How to cite this article: HU Maoshun, ZHAO Guolong, LI Liang, et al. Investigation on material response of 55% SiC_p/Al composites induced by pulsed laser[J]. Transactions of Nanjing University of Aeronautics and Astronautics, 2020, 37(S): 49-57.

http://dx.doi.org/10.16356/j.1005-1120.2020.S.007

zones and heat damage are often inevitable during LMM, which are harmful to the service performance of materials.

In recent years, micro milling has become a useful machining technique suitable for three-dimensional micro parts. In comparison with other micro-machining processes, micro milling involves controllable machining accuracy and high efficiency[8-9]. Liu et al.[10] studied the removal mechanism of micro milling of SiC_p/Al composites, pointing out that the machined surface quality was prone to be better when SiC ceramic particles were removed in the ductile regime. Liu et al.[11] reported the typical surface defects in micro milling of SiC_p/Al composites and recommended feed per tooth should be close to half of the particle size. In spite of great expectations of micro milling, tool wear and low efficiency make restrictions on further usage. On account of limitations in the fabrication of micro cutting tools, improvement of sharpness and hardness of micro cutting tools was limited. Laser assisted micro milling (LAMM) is a hybrid machining process that combines laser beam machining and micro milling[12]. Dong et al.[13] performed laser assisted micro milling and found a maximum reduction of 76% tool wear and a maximum improvement of 3.8-fold tool life in comparison with conventional micro milling. However, heat-affected zones are prone to be caused during LAMM. Besides, when the temperature decreases to a normal temperature, the machinability of materials tends to reduce.

The oxidation reaction of materials is a natural phenomenon where loose oxide layers can be generated on the surface of materials. He et al.[14] investigated the oxidation behavior of ZrB_2-SiC ceramics at 1 700 ℃ where a certain thickness of loose oxide layers could be gained. However, it took 45 min to ensure the complete oxidation of superficial materials. Another research study[15] mentioned that when materials are irradiated by a laser beam, an oxidation reaction happens quickly with the scanning of the laser beam. After an oxidation reaction, the mechanical properties of the produced oxides are irreversible. The produced oxide layers are removed by micro milling and less tool wear is found. Because of the extremely weak stiffness of oxide layers, the micro cutting tool can move in a large feed rate which results in the improvement of machining efficiency.

In this paper, a novel process called laser-induced oxidation coupled with micro milling (LOMM) is proposed for high efficient micro-milling of SiC_p/Al composites. In this study, relevant phenomena of laser-induced oxidation are investigated. Besides, the effects of reaction surrounding and laser average power on the material response of SiC_p/Al composites are studied during laser-induced oxidation.

1 Material and Methods

1.1 Workpiece materials

SiC_p/Al composites with 55% (We use 55% to denote 55% volume fraction in this paper) SiC particles as reinforcement were used as workpiece material. The microstructure of 55% SiC_p/Al composites is shown in Fig.1. The mean size of the silicon carbide particles is about 30 μm. The SiC_p/Al composites were divided by wire electrical discharge machining into samples with a size of 20 mm×4 mm×4 mm. Then, the samples went through grinding, polishing and ultrasonic cleaning.

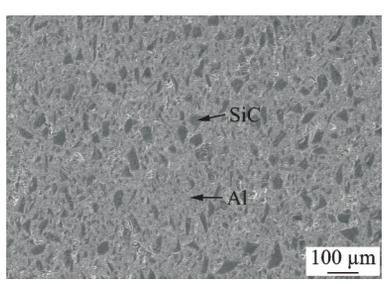

Fig.1 Microstructure of 55% SiC_p/Al composites

1.2 LOMM and laser-induced oxidation

The laser-induced oxidation experiments were carried out with a nanosecond pulsed ytterbium-doped fiber laser (YLP-1/100/20, IPG Photonics). The 3D model of the instrument is shown in Fig.2(a). Fig.2(b) presents the principle diagram and main parameters of the laser-induced oxidation apparatus. Fig.3 shows the arrangement of the work-

piece. The laser beam was focused on the surface of workpieces 1 and 2. The workpieces 1 and 2 were arranged side by side for obtaining the cross-section of the oxidation layer and sub-layer. To ensure sufficient oxidation, industrial oxygen was applied to assist the oxidation of SiC_p/Al composites. The formed oxide layer was removed by a micro end mill which was fixed at the high-speed spindle.

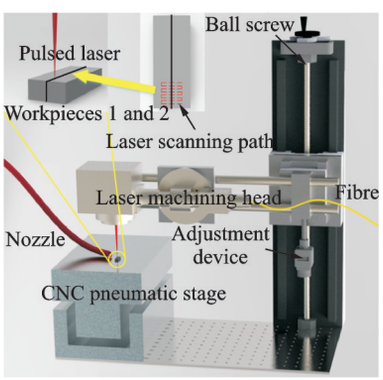

(a) 3D model

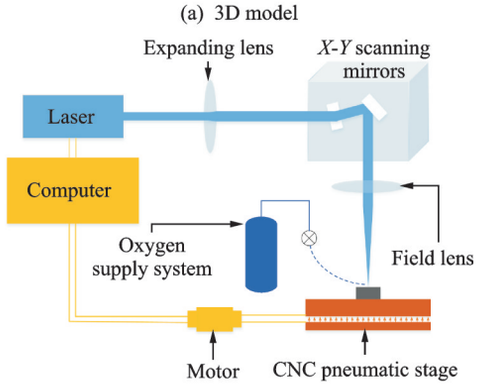

Wavelength:1 064 nm Average power:2—20 W
Pulse duration:100 ns Pulse frequency:20 kHz
Beam propagation M^2: 1.5
Input beam diameter: 7.5 mm

(b) Principle diagram of experimental equipment

Fig.2 3D model and principle diagram of experimental equipment

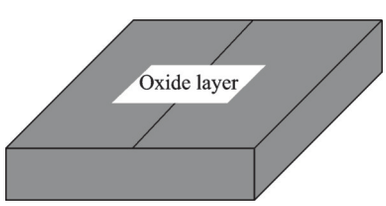

Fig.3 Arrangement of workpiece

Laser process parameters are classified into laser fluence and laser overlap rate. The laser fluence equation is shown as follows

$$F=\frac{P}{fs}=\frac{4P}{f\pi D^2} \tag{1}$$

where F is the laser fluence, P the laser average power, f the pulse frequency, and D the diameter on the focal surface.

Fig.4(a) illustrates the pulse overlap rate. Fig.4(b) demonstrates the scan overlap rate. Pulse overlap rate and scan overlap rate are described as follows, respectively

$$\delta_x=\frac{x}{D}\times 100\%=\left(1-\frac{X}{D}\right)\times 100\%=\left(1-\frac{v}{fD}\right)\times 100\% \tag{2}$$

$$\delta_y=\frac{y}{D}\times 100\%=\left(1-\frac{Y}{D}\right)\times 100\% \tag{3}$$

where δ_x is the pulse overlap rate, x the transverse overlap length, X the spot distance in the laser scanning direction, v the laser scanning speed, δ_y the scan overlap rate, y the longitudinal overlap length, and Y the spot distance between scanning tracks, namely scanning pitch.

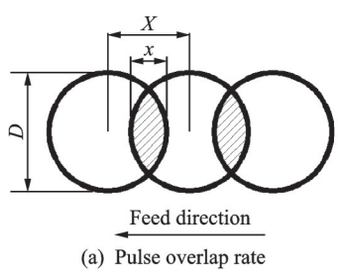

(a) Pulse overlap rate

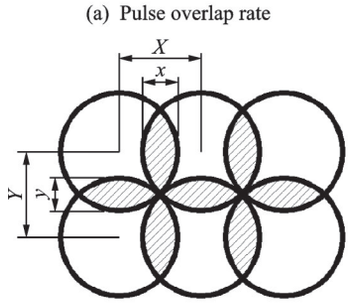

(b) Scan overlap rate

Fig.4 Schematic diagram of pulse overlap rate and scan overlap rate

In the experiments, D is 57 μm. According to Eq.(1), laser fluence is influenced by laser average power. In the same manner, pulse overlap rate and scan overlap rate are related to laser scanning speed and scanning pitch, respectively.

In this paper, f was selected as 20 kHz, v was chosen as 1 mm/s, and Y was 10 μm. The effects of reaction surrounding and laser average power on the material response of SiC_p/Al composites were

investigated. The values of laser average power were chosen to be 4, 6, 8, and 10 W.

1.3 Characterization

A scanning electron microscopy (SEM, S4800, Hitachi) equipped with an energy dispersive spectrometer (EDS) was adopted to observe the morphology of oxide layers and sub-layers and detect the elemental change. The measurement of the thicknesses of the oxide layers and the sub-layers was also performed by SEM. X-ray diffraction (XRD, D8 Advance, Bruker) was used to detect the phase composition. Cu-target ray tube was applied to scan from 10° to 80° (2θ) in a step size of 0.02° by X-ray diffraction.

2 Results and Discussion

2.1 Material response of SiC_p/Al composites under laser-induced oxidation

The contrast of the morphology of SiC_p/Al composites before and after laser scanning is presented in Fig.5. Before laser scanning, the workpiece materials are distributed with micro pores and SiC particles are embedded in the matrix. After laser scanning, the surface of the workpiece becomes loose. EDS maps of element variation are shown in Fig.6. Before laser scanning, the elements detected are shown in Fig.6(a), among which oxygen element cannot be found. In Fig.6(b), when the workpiece undergoes laser irradiation, the oxidation reaction takes place and large amounts of oxides are generated, which can be proven by oxygen element.

Oxidation reactions occur when SiC_p/Al composites are exposed to the high temperature induced by a pulsed laser. The equations of oxidation reactions are shown as follows

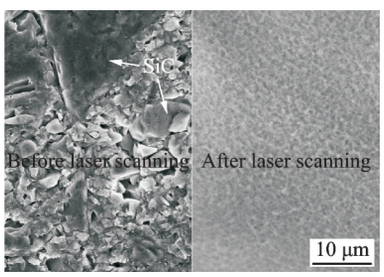

Fig.5 Morphology of SiC_p/Al composites before and after laser scanning

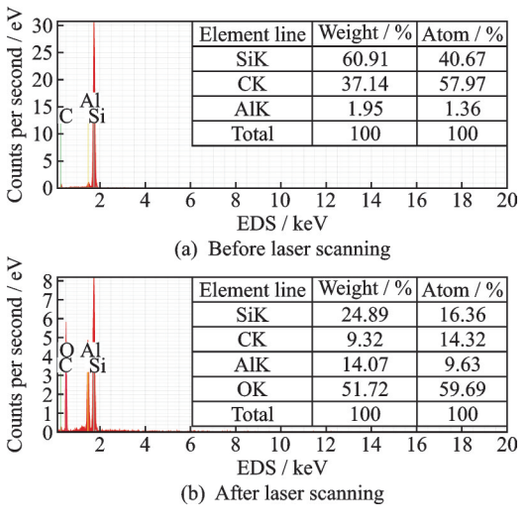

Fig.6 EDS maps before and after laser scanning

$$2SiC + 3O_2 = 2SiO_2 + 2CO \quad (4)$$

$$SiC + 2O_2 = SiO_2 + CO_2 \quad (5)$$

$$SiC + O_2 = SiO_2 + C \quad (6)$$

$$4Al + 3O_2 = 2Al_2O_3 \quad (7)$$

In addition, SiO_2 reacts with Al under high temperature. The equation is shown as follows

$$3SiO_2 + 4Al = 3Si + 2Al_2O_3 \quad (8)$$

2.2 Effect of reaction surrounding on the material response

To investigate the effect of reaction surrounding on the material response, two sets of experiments were carried out. One was in the air, the other was in an oxygen-rich atmosphere. The laser average power is 6 W, when the scanning pitch is 10 μm, the scanning speed is 1 mm/s and the pulse frequency is 20 kHz.

The morphology of oxide layers in different reaction surroundings is shown in Fig.7. Fig.7(a) is the morphology of the oxide layer produced in the air. The flocculent oxides cover the surface of the workpiece, where deep micro gaps and pores can be seen. While in Fig.7(b), the oxide layer is relatively flat and distributed with shallow micro gaps. The phenomenon manifests the promotion of oxygen in the generation of oxides.

After ultrasonic cleaning, the sub-layers appear. The morphology of sub-layers in different reaction surroundings is presented in Fig.8. As shown in Fig.8(a), the sub-layer is rugged and full of defects.

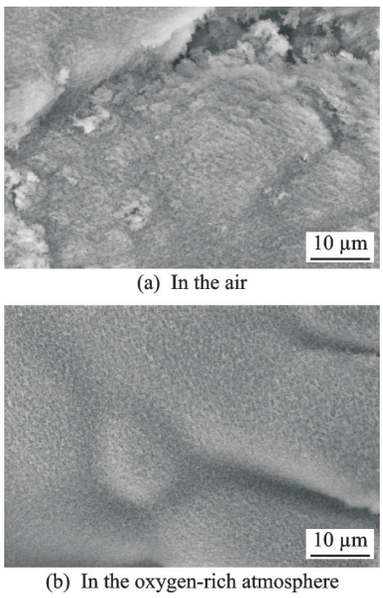

(a) In the air

(b) In the oxygen-rich atmosphere

Fig.7 Morphology of oxide layers under various reaction surroundings

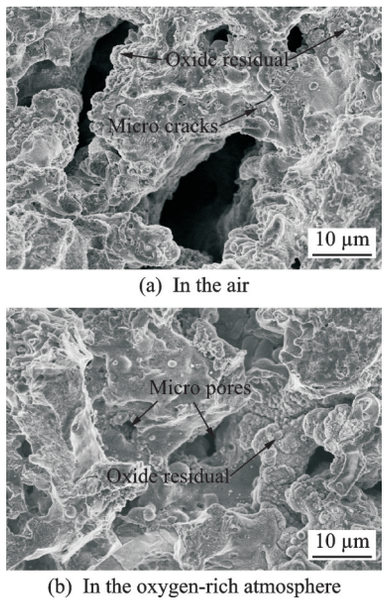

(a) In the air

(b) In the oxygen-rich atmosphere

Fig.8 Morphology of sub-layers under various reaction surroundings

In addition, a little oxide residual sticks to the surface of the sub-layer. With the loading and unloading of the pulsed laser beam, a large temperature gradient is generated, contributing to the release of the residual stress of the workpiece materials. On account of the release of residual stress, micro cracks are formed in the inner of the sub-layer and extend to the superficiality of the sub-layer. Instant high temperature caused by pulsed laser leads to the evaporation of materials and the formation of micro pores of the sub-layer. Besides, owing to the density difference between SiC and Al, SiC particles with a bigger density are prone to sink when the Al matrix gradually softens, which can be verified by pores with the size approximate to the mean size of SiC particles. In Fig.8(b), much oxide residual covers the sub-layer and fills in micro pores. Under the same parameters, sufficient oxygen supply can promote the production of oxides.

Fig.9 shows the XRD patterns of laser-induced oxidation in different reaction surroundings. Fig. 9 (a) depicts the weak diffraction peaks of oxides, which manifests that the materials are not oxidized completely. Fig.9(b) highlights several diffraction peaks of oxides, showing that the oxidation reaction takes place thoroughly. Numerous diffraction peaks of mullite ($2Al_2O_3 \cdot SiO_2$) indicate that there are numerous oxides formed in the oxidation reaction. Due to the barrier of the oxide layer, the substrate materials fail to be detected by XRD. The results show that the reaction surrounding is of great significance to the material response.

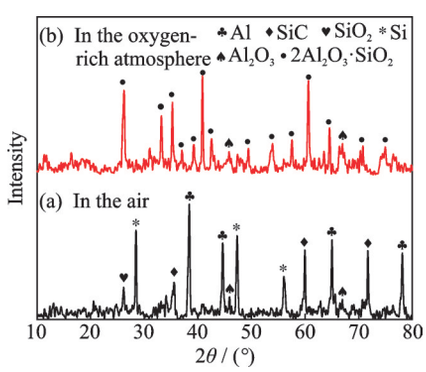

Fig.9 XRD patterns of oxide layers under different reaction surroundings

The thicknesses of oxide layers and sub-layers are the key factor that affect the material removal rate of micro milling. The cross-sections of oxide layers and sub-layers are presented in Fig.10. As displayed in Fig.10(a), oxidation reactions occur in the air. Due to insufficient oxygen, the thicknesses of the oxide layer and sub-layer are 103 μm and 17 μm. However, under an oxygen-rich environment, the laser-induced oxidation reaction is intense and large quantities of oxides pile up. Due to the

emitted heat of the oxidation reaction and the remaining heat from the laser beam, the sub-layer under an oxygen-rich atmosphere tends to be thicker than that in the air. In Fig.10(b), the thicknesses of the oxide layer and sub-layer in an oxygen-rich atmosphere are 138 μm and 21 μm which increase by 34% and 23% compared with those in the air.

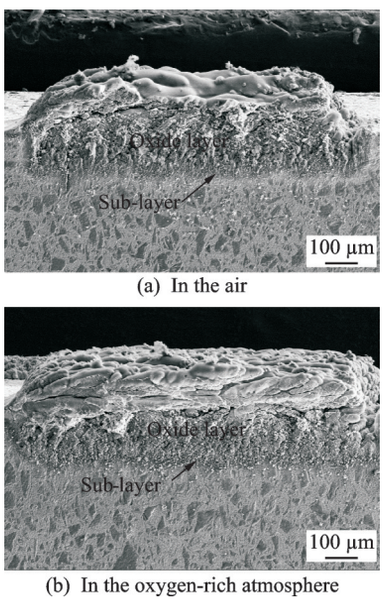

(a) In the air

(b) In the oxygen-rich atmosphere

Fig.10 Cross-sections of oxide layers and sub-layers under different reaction surroundings

Based on the above experiments and analysis, sufficient oxygen supply is beneficial to the generation of oxides. The typical features of oxide layers are loose which can be removed by micro milling without efforts. The sub-layer is rough and full of defects, which should be eliminated as finish. Therefore, laser-induced oxidation experiments should be carried out under an oxygen-rich atmosphere.

2.3 Effect of laser average power on the material response

When other laser process parameters keep stable, laser fluence increases along with the increase of laser average power. The larger the laser fluence is, the more energy absorbed by the workpiece is. Energy leads to the rise of temperature, which contributes to a more intense oxidation reaction. Nevertheless, excessive temperature induced by high laser average power causes severe heat damage.

The morphology of SiC_p/Al composites under various laser average powers is shown in Fig.11. In Fig.11(a), with the laser average power fixed at 4 W, the thin oxide layer forms on the workpiece. Owing to that the laser average power is low, oxides do not have enough energy to grow so that the oxide layer fails to cover the surface of the workpiece and is full of micro gaps. As shown in Fig.11(b), when the laser average power is 6 W, the reaction temperature increases further. Higher temperature acts as a catalyst to intensify oxidation reaction. Oxides continuously extend and cover the gaps,

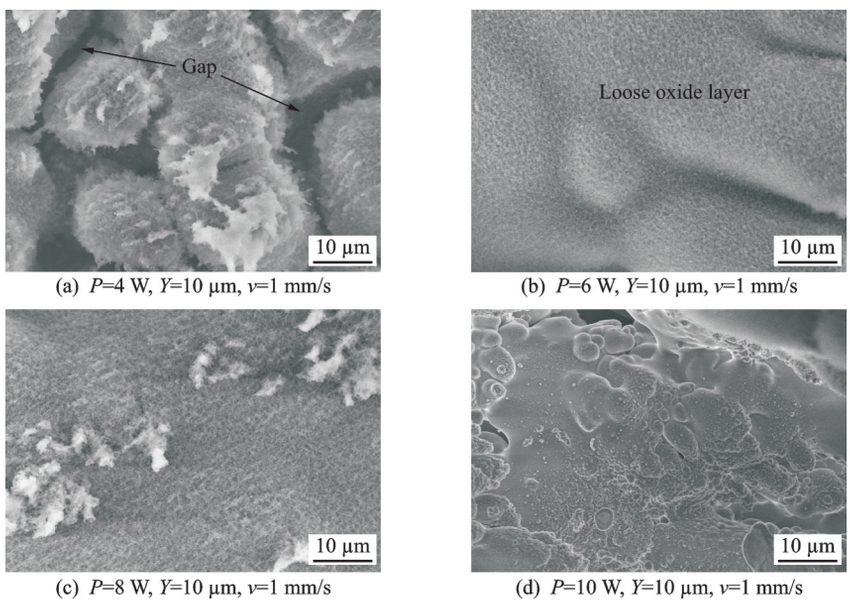

(a) P=4 W, Y=10 μm, v=1 mm/s

(b) P=6 W, Y=10 μm, v=1 mm/s

(c) P=8 W, Y=10 μm, v=1 mm/s

(d) P=10 W, Y=10 μm, v=1 mm/s

Fig.11 Morphology of oxide layer at different laser average powers

forming a loose oxide layer. As the average power reaches 8 W in Fig.11(c), the reaction temperature enables Al and SiC to react with oxygen more completely. Evident micro gaps are covered by oxides. Oxides are blown off from the surface of the oxide layer to form floccules. At this time, the oxide layer gets dense and hard, which leads to severe tool wear during micro milling. In Fig.11(d), when the average power is up to 10 W, the sub-layer starts up evaporation and melting. Parts of the molten sub-layer are expelled out on account of pressure originating from vapor and recast on the surface of the oxide layer.

The phase composition of oxide layers formed at different laser average powers is demonstrated in Fig.12. As presented in Fig.12(a), with the laser average power fixed at 4 W, there is only a weak peak of SiO_2, indicating that small amounts of oxides are formed. Owing to that the laser average power is low, the materials do not absorb enough energy to react with oxygen sufficiently. As displayed in Fig.12(b), when the laser average power is 6 W, large amounts of oxides are produced, such as SiO_2 and Al_2O_3. Based on Eq.(8), Si is also a signal product of oxidation reaction which comes from SiO_2 and Al. The oxide layer works as a layer of shielding film to make the intensity of diffraction peaks of SiC and Al diminish dramatically. In Fig.12(c), as the laser average power is up to 8 W, the oxidation reaction becomes much more intense. The diffraction peaks of SiC and Al disappear, meaning SiC and Al on the surface of materials are oxidized completely. Under high temperature, SiO_2 mobiles

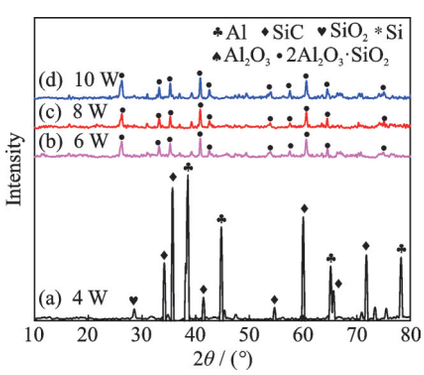

Fig.12 XRD patterns of oxide layer at different laser average powers

into other oxide phases and blends with Al_2O_3 to form considerable $2Al_2O_3 \cdot SiO_2$(mullite). In Fig.12(d), when the laser power is 10 W, the content of $2Al_2O_3 \cdot SiO_2$ oxides keeps expanding, finally covering the surface of the workpiece.

To raise the material removal rate, cutting depth is the same important. As shown in Fig.13, when the laser average power rises, the thicknesses of oxide layers and sub-layers continue to increase. As shown in Fig.13(a), when the laser average power is 4 W, the thickness of the oxide layer is thin. When the laser power reaches 6 W which is the breakdown threshold of SiC_p/Al composites, the oxide layer expands quickly. As the laser average power comes to 8 W, the oxide layer goes on expanding with a slower growth rate, which is due to the shielding effect of plasma. The maximum thicknesses of the oxide layer and sub-layer are 291 μm and 29 μm under an oxygen-rich atmosphere with the laser average power selected as 10 W. In Fig.13(b), the thickness of the sub-layer increases gradually with the increase of laser average power. When the laser average power increases all the way, oxide layers keep thickening and exhaust much energy. The remaining energy makes small amounts of the materials experience phase change, producing sub-layers whose thickness has no obvious change in general. Under an oxygen-rich atmosphere, an intense oxidation reaction releases heat to promote the production of a sub-layer. The minimum thickness of the sub-layer is 14 μm under an oxygen-rich atmosphere and 8 μm in the air, while the maximum thicknesses of that are 29 μm and 25 μm, respectively. The variety of thicknesses of oxide layers in various reaction surroundings further prove the necessity and significance of sufficient oxygen supply.

In order to raise the material removal rate of micro milling and diminish tool wear, a thicker and loose oxide layer and a thinner sub-layer are the optimum choice. When the laser average power is 6 W, the thickness of the oxide layer is 138 μm which is loose and easy to be removed. Besides, the value of the thickness of the sub-layer is just 21 μm. When the laser average power exceeds 6 W, the thickness of the sub-layer enlarges gradually. Besides, the

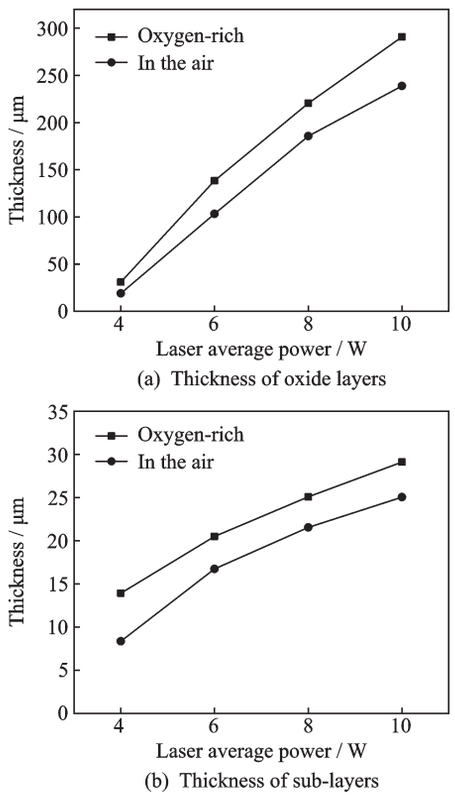

Fig.13 Variation of thicknesses of oxide layers and sub-layers under different reaction surroundings

structure of the oxide layer is not loose enough. Thus, under an oxygen-rich atmosphere, the optimum value of laser average power is 6 W.

3 Conclusions

(1) Laser-induced oxidation experiments were conducted on the 55% SiC_p/Al composites utilizing a nanosecond pulsed laser (YLP-1/100/20). Under the irradiation of a nanosecond pulsed laser beam, loose oxide layers and sub-layers are produced on the surface of the workpiece.

(2) Oxidation reaction surroundings have a vital impact on the morphology and thickness of the oxide layer. Exposed to an oxygen-rich atmosphere, the expanding percentage of the oxide layer approximately ranges from 20% to 60%. The micro gap of the thickness of sub-layers in different reaction surroundings manifests that oxygen has a minor effect on the thickness of the sub-layer.

(3) There is an obvious positive correlation between the thickness of the oxide layer and the laser average power. When the laser average power increases from 4 W to 6 W, the thickness of the oxide layer increases significantly. As the laser average power increases, the sub-layers also get thicker slightly.

(4) To acquire a thicker oxide layer and a thinner sub-layer, within the experimental parameters, the laser average power of 6 W is the optimum parameter. In addition, sufficient oxygen supply is a necessity. Under this condition, the thicknesses of the oxide layer and sub-layer are 138 μm and 21 μm, respectively.

References

[1] LIU Q Y, WANG F, WU W W, et al. Enhanced mechanical properties of SiC/Al composites at cryogenic temperatures[J]. Ceramics International, 2019, 45(3): 4099-4102.

[2] ATTIA U M, ALCOCK J R. Fabrication of ceramic micro-scale hollow components by micro-powder injection moulding[J]. Journal of the European Ceramic Society, 2012, 32(6): 1199-1204.

[3] ZHAO G L, HU M S, LI L, et al. Enhanced machinability of SiC_p/Al composites with laser-induced oxidation assisted milling[J]. Ceramics International, 2020, 46(11): 18592-18600.

[4] WANG Z L, GENG X S, CHI G X, et al. Surface integrity associated with SiC/Al particulate composite by micro-wire electrical discharge machining[J]. Materials and Manufacturing Processes, 2014, 29(5): 532-539.

[5] HAGHBIN N, SPELT J K, PAPINI M. Abrasive waterjet micro-machining of channels in metals: Comparison between machining in air and submerged in water[J]. International Journal of Machine Tools & Manufacture, 2015, 88: 108-117.

[6] CHEN T H, FARDEL R, ARNOLD C B. Ultrafast z-scanning for high-efficiency laser micro-machining[J]. Light: Science & Applications, 2018, 7: 1-9.

[7] ZHAO J S, ZHANG H, YUAN L X, et al. Theoretical and experimental investigation of laser milling assisted with jet electrochemical machining[J]. Transactions of Nanjing University of Aeronautics and Astronautics, 2014, 31(5): 492-497.

[8] LIOW J L. Mechanical micromachining: A sustainable micro-device manufacturing approach[J]. Journal of Cleaner Production, 2009, 17(7): 662-667.

[9] WANG T, WAN Y, KOU Z J, et al. Micro-milling of pyramid structured surface for implant application[J]. Transactions of Nanjing University of Aeronautics and Astronautics, 2017, 34(4): 357-362.

[10] LIU J W, CHENG K, DING H, et al. An investigation of the influence of phases' removal ways on surface quality in micro milling SiC_p/Al composites[J]. Procedia CIRP, 2018, 71: 59-64.
[11] LIU J W, CHENG K, DING H, et al. An investigation of surface defect formation in micro milling the 45% SiCp/Al composites[J]. Procedia CIRP, 2016, 45: 211-214.
[12] MELKOTE S, KUMAR M, HASHIMOTO F, et al. Laser assisted micro-milling of hard-to-machine materials[J]. CIRP Annals-Manufacturing Technology, 2009, 58(1): 45-48.
[13] DONG X Y, SHIN Y C. Improved machinability of SiC/SiC ceramic matrix composite via laser-assisted micromachining[J]. International Journal of Advanced Manufacturing Technology, 2017, 90 (1/2/3/4): 731-739.
[14] HE J B, WANG Y G, LUO L, et al. Oxidation behaviour of ZrB_2-SiC (Al/Y) ceramics at 1700 ℃[J]. Journal of the European Ceramic Society, 2016, 36: 3769-3774.
[15] YANG Y F, ZHAO G L, HU M S, et al. Fabrication of CVD diamond micro-milling tool by hybrid machining of laser-induced graphitization and precision grinding[J]. Ceramics International, 2019, 45(18): 24127-24136.

Acknowledgements This work was supported by the National Natural Science Foundation of China (Nos.51705249, 52075255), the China Postdoctoral Science Foundation (No.2019M661823).

Authors Mr. **HU Maoshun** received his B.S. degree of Mechanical Engineering from Yangzhou University, Yangzhou, China, in 2018. In September 2018, he joined the Advanced Cutting Technology Research Group of College of Mechanical and Electrical Engineering from Nanjing University of Aeronautics and Astronautics (NUAA). His research topic is laser-induced oxidation assisted milling.

Dr. **ZHAO Guolong** received the B.S. and Ph.D. degrees of Mechanical Engineering from Shandong University, Jinan, China, in 2009 and 2015, respectively. From 2013 to 2014, he was a Visiting Scholar in the Department of Material Science and Engineering, University of Delaware, Delaware, USA. In June 2015, he joined NUAA. He is an associate professor of College of Mechanical and Electrical Engineering, NUAA. His research interests include advanced cutting technology, high performance cutting of composite materials, micro machining and micro-tool technology.

Author Contributions Mr. **HU Maoshun** conducted the experiments and analysis and wrote the manuscript. Dr. **ZHAO Guolong** designed the study, revised and modified the manuscript. Prof. **LI Liang** contributed to the discussion and background of the study. Mr. **ZHANG Xiaohui** and Mr. **ZHANG Kaihu** provided the workpiece material. Dr. **ZHAO Wei** provided assistance for data analysis. All authors commented on the manuscript draft and approved the submission.

Competing interests The authors declare no competing interests.

(Production Editor: XU Chengting)

55% SiC_p/Al复合材料的脉冲激光诱导行为研究

胡茂顺[1]，赵国龙[1]，李　亮[1]，张孝辉[2]，张开虎[2]，赵　威[1]
(1.南京航空航天大学机电学院，南京 210016，中国；2.北京卫星制造厂有限公司，北京 100094，中国)

摘要：碳化硅颗粒增强铝基复合材料(SiC_p/Al复合材料)被广泛应用于众多工业领域，如航空、航天以及电子封装。但是，加工效率低、刀具磨损严重以及表面质量差在SiC_p/Al复合材料加工中较为严重。激光诱导氧化能够改善SiC_p/Al复合材料的加工性。本文研究了55%(体积分数)SiC_p/Al复合材料的脉冲激光诱导行为，生成由氧化层和亚表层组成的变质层；研究了反应环境和激光平均功率对氧化层和亚表层的微结构和厚度的影响。试验结果表明，在富氧氛围中能够形成更厚的氧化层和亚表层；氧化物主要由$2Al_2O_3$•SiO_2(莫来石)组成；激光平均功率和氧化层及亚表层的厚度之间存在正相关的关系；当激光平均功率为6 W、激光扫描间距为10 μm、激光扫描速度为1 mm/s且反应处于富氧氛围中时，形成了138 μm厚的疏松氧化层和21 μm厚的亚表层；激光诱导氧化能够实现SiC_p/Al复合材料的高效加工。

关键词：微结构；氧化行为；SiC_p/Al复合材料；脉冲掺镱光纤激光器